Improvement of Infrared Imaging Video Bolometer for Application to Deuterium Experiment on the Large Helical Device[a)]

K. Mukai,[1,2,b)] R. Abe,[3] B. J. Peterson,[1,2] and S. Takayama[1]

[1]*National Institute for Fusion Science, National Institutes of Natural Science, Toki 509-5292, Japan*
[2]*SOKENDAI (The Graduate University for Advanced Studies), Toki 509-5292, Japan*
[3]*National Institute of Technology, Sendai College, Natori 981-1239, Japan*

(Presented XXXXX; received XXXXX; accepted XXXXX; published online XXXXX)
(Dates appearing here are provided by the Editorial Office)
An Infrared imaging video bolometer was improved for the application to a neutron environment in fusion plasma devices, i.e., the Large Helical Device (LHD). In order to calibrate the thermal characteristics of the activated foil absorber inside the plasma vacuum vessel, the remote-controlled in-situ calibration system was improved with high-surface-flatness mirrors. Furthermore, the carbon coating method was improved by introducing a vacuum evaporation technique instead of the conventional spray technique to realize the coating on both sides of the absorber with reproducibility and uniformity. The optimal thickness of the coating was also determined. Owing to these coating improvements, the reproducibility of the effective emissivity on both sides especially was improved. Finally, the variation with neutron irradiation of the thermal characteristics of the foil absorber was investigated. It was found that the effect was not significant for the total neutron emission of 3.6×10^{18} on LHD.

I. INTRODUCTION

Plasma radiation measurement is one of the fundamental measurements in plasma fusion research. The InfraRed imaging Video Bolometer (IRVB) is a powerful tool for multi-dimensional measurement, which is required for the plasma radiation measurement since the radiation mainly occurs outside the last closed flux surface where axis symmetry cannot be assumed. The IRVB has been developed in the Large Helical Device (LHD) [1, 2]. The IRVB has a combined structure of a pinhole camera with a metal foil absorber and an InfraRed (IR) camera. Plasma radiation through a pinhole is projected onto the foil absorber. The temperature rise of the foil is observed from the backside using the IR camera. Here, the absorber is coated on both sides to increase the absorption of the plasma radiation and the infrared signal to the IR camera. The foil absorber is divided into bolometer pixels numerically. In LHD, the size of the platinum (Pt) absorber is 130 mm × 100 mm × 2.5 μm (thickness) and the absorber is divided into the bolometer pixel with the size of 10 mm × 10 mm in the numerical analysis. The IRVB has been installed in LHD [1, 2], JT-60U [3], KSTAR [4], HL-2A [5], and Alcator C-mod [6]. The IRVB plays an important role in investigating the plasma radiation phenomena, i.e., plasma detachment and radiation collapse. In LHD, clearly different radiation profiles were observed between the neon-seeded plasmas and the krypton-seeded plasmas [7]. In KSTAR, the radiation profiles were observed in krypton-seeded plasmas with an internal transport barrier [4].

In order to apply the IRVB to a reactor plasma, i.e., ITER, countermeasures against neutron irradiation are required. In LHD, the deuterium experiment was started in 2017. The maximum neutron emission rate was 3.3×10^{15} /s in the first deuterium experimental campaign. The countermeasures of the IRVB in LHD can be classified into roughly two problems: (i) neutron shielding for the IR camera and (ii) in-situ calibration of the thermal characteristics of the foil absorber. The neutron shielding has already been designed based on the operation experience in JT-60U [3], and the IR camera could be operated during the first deuterium experimental campaign. Then, we present the in-situ thermal characteristics calibration technique in this paper. In Section II, an improved laser injection system for the activated foil absorber inside the plasma vacuum vessel is described. In Section III, a carbon coating technique with reproducibility and uniformity is presented. This is required in association with the in-situ calibration system. Variation of the thermal characteristics of the foil absorber in a neutron environment is discussed in Section IV.

II. IMPROVEMENT OF IN-SITU CALIBRATION SYSTEM

The temperature profile on the foil absorber observed using the IR camera cannot be directly convert to the plasma radiation profile since the absorbed plasma radiation

[a)]Published as part of the Proceedings of the 22nd Topical Conference on High-Temperature Plasma Diagnostics (HTPD 2018) in San Diego, California, USA.
[b)]Author to whom correspondence should be addressed: mukai.kiyofumi@nifs.ac.jp

diffuses in the foil. Therefore, the incident plasma radiation profile on the foil absorber is solved for from the foil temperature profile by using the two-dimensional heat diffusion equation (Eq. (1) [8].

$$-\frac{P_{\mathrm{rad}}}{k_{\mathrm{eff}}t_{\mathrm{f}}l^2}+\frac{\varepsilon_{\mathrm{eff}}\sigma_{\mathrm{S-B}}(T^4-T_0^4)}{k_{\mathrm{eff}}t_{\mathrm{f}}}+\frac{1}{\kappa_{\mathrm{eff}}}\frac{\partial T}{\partial t}=\frac{\partial^2 T}{\partial x^2}+\frac{\partial^2 T}{\partial y^2}, \quad (1)$$

Here, P_{rad} is the absorbed plasma radiation, l is the size of the bolometer pixel, $\sigma_{\mathrm{S-B}}$ is Stefan-Boltzmann coefficient, T is absorber temperature, and T_0 is background temperature. Since we handle the three-layered structure (carbon - platinum - carbon) as a single material, its thermal characteristics are calibrated at every bolometer pixel as effective values: $\varepsilon_{\mathrm{eff}}$ is effective emissivity, k_{eff} is the effective thermal conductivity, and κ_{eff} is the effective thermal diffusivity. The variation of the foil thickness, t_{f}, is included in k_{eff} since t_{f} appears with k_{eff} in Eq. (1).

When the foil absorber becomes radioactive, the calibration inside the plasma vacuum vessel itself is required due to constraints on the removal of radioactive materials from the controlled area. Therefore, an in-situ calibration system was designed [8]. The advantage of the previous system is that the number of optics is minimized by using a hot mirror (Edmund Optics/#64-472 45◦ 101 × 127). However, since the hot mirror surface flatness of 4 - 6 λ is larger than the normal mirrors, there is room for improvement. FIG. 1 shows the schematic of the improved in-situ calibration system. The laser injection unit is removable in order to reduce the amount of the activated components. A He-Ne laser (JDS Uniphase/1145, 632.8 nm × 22.5 mW) is irradiated from outside the vacuum vessel

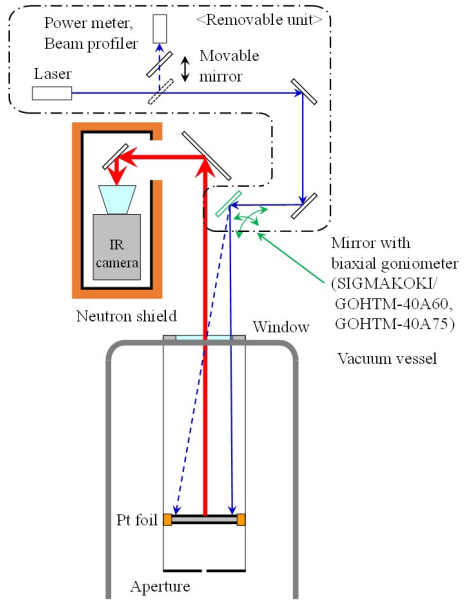

FIG. 1. Schematic of in-situ calibration system for the thermal characteristics of foil absorber. Blue-thin (solid and dashed) arrows indicate paths of visible light from a He-Ne laser, red-thick arrows indicate the path of the infrared signal from the heated foil absorber to the IR camera, respectively.

after checking the beam profile and power. The transmittance of the ZnSe window for the laser is ~ 83%. The irradiation position can be scanned using a mirror with two motorized goniometers (SIGMAKOKI/GOHTM-40A60/GOHTM-40A75) and LabVIEW. The accuracy of the irradiation position is better than 0.7 mm. The mirror is located outside the IR camera (FLIR/SC655) field of view for the foil absorber by considering the angle of view. The IR signal from the heated foil absorber is detected using two mirrors. The transmittance of the ZnSe window for the IR signal is > 95%. Since the surface flatness of these mirrors are λ/10, the scattering of the image due to the hot mirror was removed.

III. IMPROVEMENT OF CARBON COATING TECHNIQUE ON FOIL ABSORBER

A. Carbon coating with reproducibility and uniformity using evaporation technique

For the in-situ calibration using the laser injection system described in Section II, the laser must be irradiated from the side opposite the plasma radiation. Then, a carbon coating with reproducibility and uniformity is required on both sides of the foil absorber. Here, the reproducibility and the uniformity mean that the temperature profile on the foil absorber can be reproduced regardless of the laser irradiation direction and the laser irradiation position, respectively. In the previous study, the reproducibility of the coating was improved by introducing an evaporation coating technique [8]. Hence, in this study, the foil absorber samples were increased in size from a diameter of ϕ = 16.3 mm to ϕ = 37 mm and the uniformity of the carbon was confirmed. The sample sizes correspond to the foil holder of oxygen free copper.

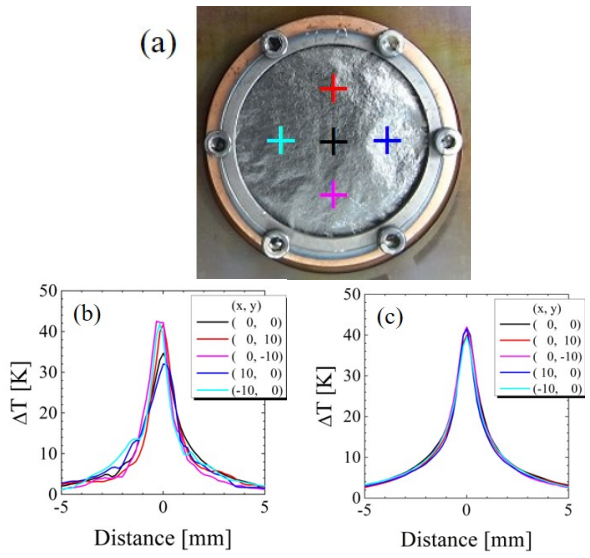

FIG. 2. (a) Sample of foil absorber and laser irradiation points. Profiles of temperature increase due to laser irradiation on (b) spray coated and (c) evaporation coated samples.

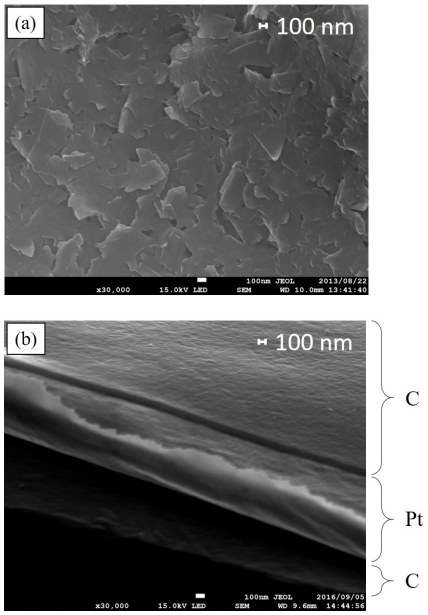

FIG. 3. SEM images (× 30,000) of carbon surface structure on (a) spray coated sample and (b) evaporation coated sample.

A sample of Pt foil absorber was coated using a vacuum coater (ULVAC KIKO/VPC-260F). A carbon rod of $\phi = 0.9$ mm was resistively heated by ~ 30 A in a vacuum of < 10 Pa. After the coating, a He-Ne laser (632.8 nm, 12.6 mW) irradiated the samples in vacuum. Then, the temperature profile on the backside of the laser irradiation was observed using an IR camera. The laser irradiation point was scanned as shown in FIG. 2 (a): center of the absorber and four locations 10 mm from the center of the absorber (top, bottom, left, and right). The profiles of temperature increase observed for the five irradiation positions on spray and evaporation coated samples were over-plotted in FIG. 2 (b) and (c), respectively. Higher uniformity coating was successfully realized using the evaporation technique. FIG. 3 shows the surfaces of the carbon coating observed by a scanning electron microscope (SEM, JEOL/JSM-7100F). The uniformity of the surface structure with the evaporation coating provide the uniformity of the temperature profile.

B. Optimal carbon thickness for carbon coating

Since the thickness of the carbon coating became controllable by introduction of the evaporation technique, its optimal thickness was determined. When the thickness is too thin, the absorption of the plasma radiation will decrease. On the other hand, when the thickness is too thick, the Pt foil of 2.5 μm thickness which is not sufficiently strong mechanically may be torn. Since the thickness that can be coated by one evaporation process is only approximately 20 nm, a large number of evaporation processes are needed for the thicker coating. The repetition of the evacuation and the venting can cause small cracks in the absorber. The cracks lead to non-uniformity of the thermal propagation in the absorber. Therefore, the number of coating cycles should be minimized to protect the foil absorber.

Here, Pt foils of 10 μm thickness and a ND:YAG laser (HCP/GLMP-0100A, 532 nm, ~100 mW) were used to remove the effect of small pinholes in the 2.5 μm Pt foil. The coating thickness can be measured using a deposition controller (ULVAC KIKO/ CRTM-6000G) and a film thickness sensor (ULVAC KIKO/ CRTS-4). However, the position of the sensor varies from that of the foil absorber. Hence, the coating thickness was evaluated by the SEM observation shown in FIG. 3 (b) and the displayed thickness on the deposition controller was calibrated as shown in FIG. 4. The calibrated coating thickness dependence of the temperature increase is shown in FIG. 5. The temperature increase saturated when the coating thickness was larger than 160 nm. Then, 160 nm was determined as the optimal thickness of the carbon coating.

C. Thermal characteristics reproducibility of foil absorber on both sides

Laser irradiation direction dependence of the thermal characteristics was compared between evaporation and spray coated absorbers (130 mm × 100 mm). This calibration experiment was performed in a test vacuum chamber [9, 10]. Firstly, the He-Ne laser irradiated the plasma side of the foil absorber and the temperature profile was observed from the camera side using an IR camera (FLIR/SC4000). Secondly, the laser irradiated the camera side of the absorber and the temperature profile was observed from the plasma side. Evaluated k_{eff}, $\varepsilon_{\mathrm{eff}}$, and κ_{eff} profiles are shown in FIG. 6, 7, and 8, respectively, as comparisons of the laser irradiation direction and coating method. The errors were determined as Eq. (2).

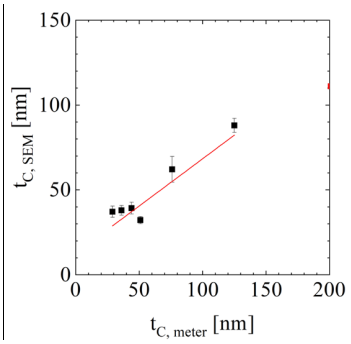

FIG. 4. Relationship of carbon thickness between film thickness sensor measurement and SEM observation.

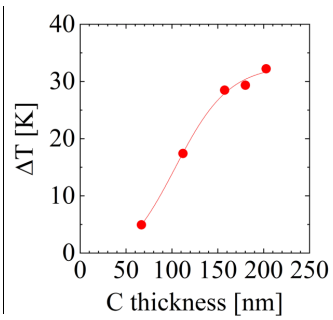

FIG. 5. Dependence of temperature increase ΔT as a function of carbon coating thickness.

$$\text{Error} = \frac{\left|P_{\text{Camera}} - P_{\text{Plasma}}\right|}{2} \Bigg/ \left(\frac{P_{\text{Camera}} + P_{\text{Plasma}}}{2} \right), \qquad (2)$$

Here, P_{Camera} and P_{Plasma} are parameters evaluated by the laser irradiation from the camera side and plasma side, respectively. The errors of k_{eff} between both directions were

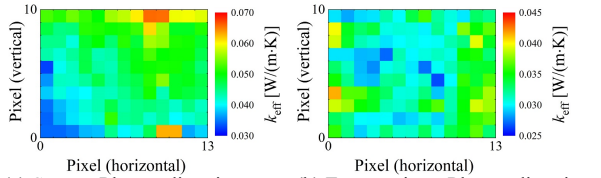

(a) Spray - Plasma direction (b) Evaporation - Plasma direction

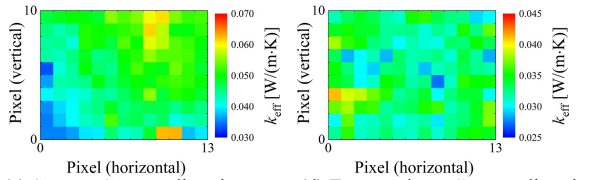

(c) Spray - Camera direction (d) Evaporation - Camera direction

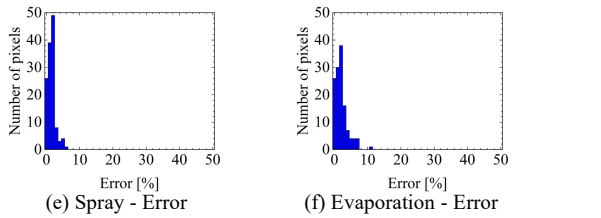

(e) Spray - Error (f) Evaporation - Error

FIG. 6. Laser irradiation direction dependence of effective thermal conductivity k_{eff} profile and the error profile between the two directions in spray coated (a, c) and evaporation coated (b, d) foil absorbers. Error distribution in spray coated (e) and evaporation coated (f) foil absorbers.

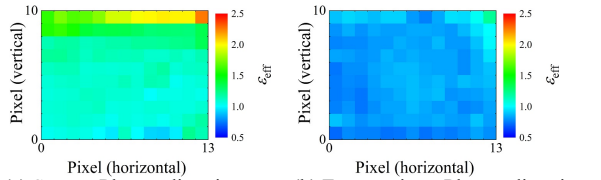

(a) Spray - Plasma direction (b) Evaporation - Plasma direction

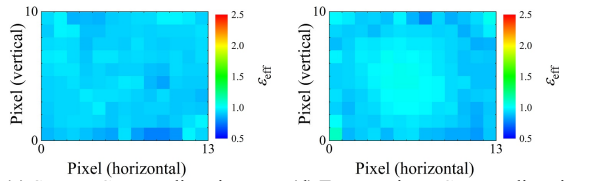

(c) Spray - Camera direction (d) Evaporation - Camera direction

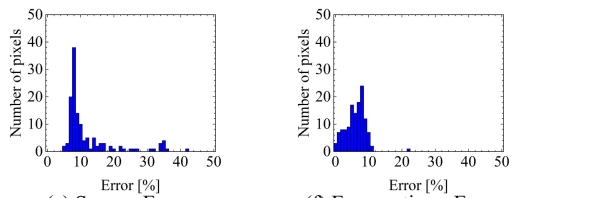

(e) Spray - Error (f) Evaporation - Error

FIG. 7. Laser irradiation direction dependence of effective emissivity ε_{eff} profile between the two directions in spray coated (a, c) and evaporation coated (b, d) foil absorbers. Error distribution in spray coated (e) and evaporation coated (f) foil absorbers.

< 7% for almost all pixels in both coatings. On the other hand, the errors of ε_{eff} between both directions in evaporation coated absorber were clearly lower than the errors in spray coated absorber. Although the ε_{eff} errors were < 10% for almost all pixels in evaporation coated absorber, the maximum ε_{eff} error was 42 % in the spray coated absorber. The coating at around the higher ε_{eff} in the spray coated absorber seemed to be thicker than at other places. The thicker spray coating with the flaky structure as shown in FIG. 3. (a) probably increased the ε_{eff}. The non-uniformity of the carbon coating thickness in the spray coated absorber was improved using the evaporation coating. In addition, the flaky surface structure in the spray coated absorber was also avoided using the evaporation coating as shown in FIG. 3. (b). The errors of κ_{eff} between both directions were < 10% for almost all pixels in both coatings. κ_{eff} errors in the evaporation coated absorber were larger than those in the spray coated absorber. However, the errors in the evaporation coated absorber possibly decreased by the improvement of the fitting process in Ref. [11] Fig. 8.

IV. VARIATION OF FOIL THERMAL CHARACTERISTICS IN NEUTRON ENVIRONMENT

A. Procedure of in-situ calibration experiment

The procedure of in-situ calibration for thermal characteristics of the foil absorber is as follows:

- Install the laser injection unit;
- Measure beam profile and power of the He-Ne laser;

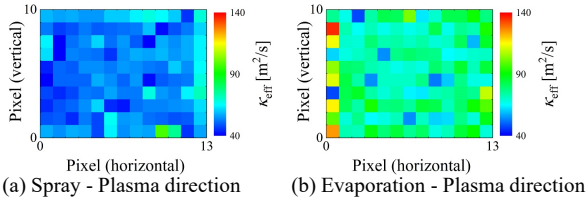

(a) Spray - Plasma direction (b) Evaporation - Plasma direction

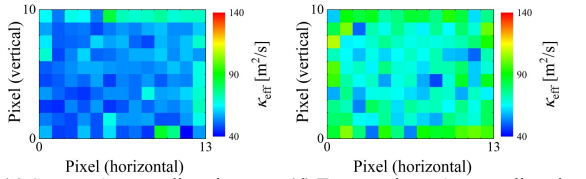

(c) Spray - Camera direction (d) Evaporation - Camera direction

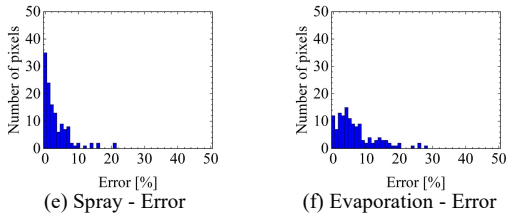

(e) Spray - Error (f) Evaporation - Error

FIG. 8. Laser irradiation direction dependence of effective thermal diffusivity κ_{eff} profile and the error profile between the two directions f in spray coated (a, c) and evaporation coated (b, d) foil absorbers. Error distribution in spray coated (e) and evaporation coated (f) foil absorbers.

- Measure coordinate (pulse number of stepping motors) at the corners of the foil absorber;
- Calculate the coordinate of the irradiation points for scanning;
- Perform in-situ calibration experiment. This procedure is fully automated by LabVIEW;
- Exit from the LHD torus hall;
- After finishing the in-situ calibration experiment (~ four hours), enter the torus hall and remove the laser injection unit.

In LHD, the in-situ calibration system was developed as a removable unit to reduce the amount of activated components. But this procedure can be controlled completely by remote when the IRVB diagnostics will be applied to ITER.

B. Variation of thermal characteristics in LHD deuterium experiment

In-situ calibration experiment of the thermal characteristics using the laser injection unit was performed three times during the experimental campaign: (1) before the deuterium experiment, (2) in the middle of deuterium experiment, and (3) after the deuterium experiment. Here, these calibration experiments were performed without plasma and magnetic field. The total neutron emission was 3.6×10^{18} for the first deuterium experimental campaign on LHD. Since the calibration method shown in Section III. C. is time-consuming, temperature increase ΔT from the background using laser irradiation was used as a simple reference for the variation of the thermal characteristics. FIG. 9 (a), (c), and (e) show the ΔT profiles for experiments (1) - (3), respectively. All ΔT profiles basically corresponds to the $\varepsilon_{\mathrm{eff}}$ profile shown in FIG. 7 (d). We should note that a tiny structure was observed from the beginning of the experimental campaign as shown in FIG. 9 (b). The differences of ΔT from before the deuterium experiment were < 15% for almost all pixels in all times. The main reason for the errors can be considered as low resolution of the IR camera. Since only ~ 8% of full pixels (640 × 480) can be used for the foil observation, additional optics can provide more accurate calibration.

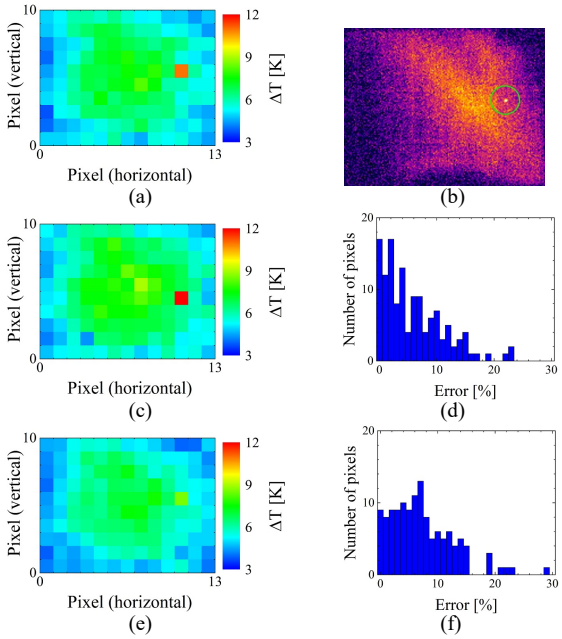

FIG. 9. Temperature increase ΔT profile due to laser irradiation to each bolometer pixel (a) before deuterium experiment. At the point where the highest ΔT was observed, a tiny structure was observed in the plasma experiment (b). ΔT profile and error distribution in middle of deuterium experiment (c, d) and after deuterium experiment (e, f). Error was evaluated as the absolute value of the difference from the first in-situ calibration (a).

V. SUMMARY

An infrared imaging video bolometer was applied to the neutron environment in LHD. In order to calibrate the thermal characteristics of the activated foil absorber inside the plasma vacuum vessel, a carbon coating on both sides was realized with reproducibility and uniformity using the vacuum evaporation technique instead of the spray coating. The reproducibility of the effective emissivity on both sides was especially improved by the evaporation coating. The variation of the thermal characteristics of the foil absorber was investigated before and after the neutron irradiation of 3.6×10^{18} on LHD. It was found that the effect was not significant. The fact that there was no shutter on the IRVB and therefore the foil was subjected to both neutrons, gammas, and plasma radiation from experiments and glow discharge cleaning indicates that the effect of these on the foil thermal characteristics is also negligible. The remote-controlled in-situ calibration technique and the coating technique should be applicable to other fusion devices.

ACKNOWLEDGMENTS

This work was supported by JSPS KAKENHI Grant Number JP17K14900 and by NIFS/NINS Grant Number NIFS16ULHH026. The authors thank the following collaborators for their excellent technical support; D. Abe (National Institute of Technology, ICHINOSEKI KOSEN), H. Makino (National Institute of Technology, Akashi College), Y. Umemura (Kanagawa Univ.), and A. Koyama (Kyushu Univ.).

[1]B. J. Peterson, Rev. Sci. Instrum. **71**, 3696 (2000).
[2]K. Mukai, B. J. Peterson, S. N. Pandya, R. Sano, and M. Itomi, Plasma Fusion Res. **9**, 3402037 (2014).
[3]B. J. Peterson *et al*., J. Nucl. Mater. **412**, 363 (2007).
[4]J. Jang *et al*., Curr. Appl. Phys. **18**, 461 (2018).
[5]J. M. Gao *et al*., Rev. Sci. Instrum. **85**, 043505 (2014).
[6]M.L. Reinke *et al*., submitted to Rev. Sci. Instrum. (2018).
[7]K. Mukai *et al*., Nucl. Fusion **55**, 083016 (2015).
[8]B. J. Peterson *et al*., Rev. Sci. Instrum. **79**, 10E301 (2008).
[9]K. Mukai, B. J. Peterson, S. Takayama, and R. Sano, Rev. Sci. Instrum. **87**, 11E124 (2016).
[10]R. Sano, *et al*., Plasma Fusion Res. **7**, 2405039 (2012).
[11]S. N. Pandya *et al*., Rev. Sci. Instrum. **85**, 054902 (2014).
[12]R. Sano *et al*., Plasma Fusion Res. **6**, 2406076 (2011).